Automatic Detection of Pigmented Network in Melanoma Dermoscopic Images

Ahmed Ayoub[1], András Hajdu[2] and Arpád Nagy[2]

[1]Benha University, Faculty of Engineering at Benha
Benha 13512, Egypt
and
Shaqra University, Faculty of Science and Arts,
Shaqra 11961, Saudi Arabia
asayub@su.edu.sa

[2]University of Debrecen, Faculty of Informatics,
4010 Debrecen, PO. Box. 12., Hungary
hajdu.andras@inf.unideb.hu, apri0912@freemail.hu

Abstract: *We present a method to automatically detect and classify the dermoscopic structure pigment network which may indicate early melanoma in skin lesions. The network is located as darker areas constituting a mesh, as well as lighter areas representing the 'holes' which the mesh surrounds. After comparing 5 methods of segmentations with the manual one, we apply a LoG filter followed by a classification algorithm to discriminate between holes belong to pigmented network from others. Then, we define an adaptive maximum distance threshold to visualize the network. The pigmented network in a lesion is classified as present or absent. We validate our method over a real-world dataset consisting of 100 images and achieve an accuracy of 70.8%.*

Keywords: Automatic Melanoma Diagnosis, Pigmented Network, Feature Extraction

1. Introduction

In a recent review of the literature data [1], the sensitivity of computer-based devices for melanoma diagnosis varied between 80% and 100% and specificity between 47% and 92%. These figures suggested that the accuracy of computer-based diagnosis does not differ significantly from that of the clinical diagnosis. Moreover, it is unrelated to the optical method of acquisition in operation.

The clinical diagnosis of melanoma is commonly based on the ABCD rule, which is a checklist of important parameters [2]. This technique focuses on asymmetry, irregular border, number of colors (associated also to slate blue veil and whitish veil), and the presence of differential structures (streaks, globular elements, etc.). This guideline requires computing a weighted score of these features. The parameter *evolution* is usually considered, becoming the "ABCDE rule".

Another method was proposed by Menzies and co-workers in 1996 [3] It is based on features such as the presence of irregular border, irregular pigmented network, abrupt cut-off of the network, streaks, globular elements and colors.
Therefore, according to the mentioned methods, melanomas usually have features indicating their melanocytic origin: pigment network; aggregated brown, or black globules; and site-specific features (e.g. parallel pattern on palms and soles, follicular openings on facial skin).

Referring to Maglogiannis et. al. [4], only 9% of the literature addresses feature distribution. A typical *pigment network* (PN) is one of these crucial features. The PN seen in melanocytic lesions stems from increased melanin content in keratinocytes or melanocytes outlining the rete ridges pattern of the epidermis. The holes in the network correspond with the epidermal suprapapillary plates [5, 6].

A typical PN, Figure 1b, is defined as "a light-to-dark-brown network with small, uniformly spaced network holes and thin network lines distributed more or less regularly throughout the lesion and usually thinning out at the periphery" [7].

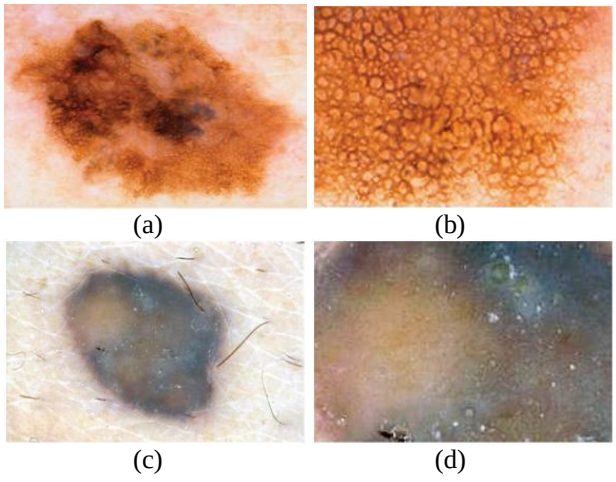

Figure 1: a) Present: A lesion containing a pigment network. b) An enlarged pigment network . c) Absent: An image of a lesion without pigment network. (d) a magnification of (c).

Automatic detection of pigment network has been investigated recently. Anantha et al. [8] propose two algorithms: one involves statistics over neighboring gray-level dependence matrices; the other involves filtering with Laws energy masks. Various Laws masks are applied and the

Received 12/2, Reviewed 12/19

responses are squared. Improved results are obtained by a weighted average of two Laws masks whose weights are determined empirically. Classification of these tiles shows approximately 80% accuracy.

Betta et al. [9] begin with taking the difference of an image and its response to a median filter. Followed by a threshold of such difference image to create a binary mask which undergoes a morphological closing operation to remove any local discontinuities. Then, this mask is combined with another created from a high-pass filter applied in the Fourier domain to exclude any slowly modulating frequencies. Results are reported graphically, appear to achieve a sensitivity of 50% with a specificity of 100%.

In 2006, Grana et al. [10] proposed a modified approach to detect and localize network patterns. Such texture is automatically detected with Gaussian derivative kernels and Fisher linear discriminant analysis; line closure and thinning is provided by morphological masking and line luminance profile fitting provides width estimation. An overall 88.3% network detection performance is reported. Even though high contrast images are used to visualize results of the method, there are false positives which are hair lines or noise. They could consider spatial arrangements of network holes to remove false positives.

Serrano et. al. [11] presented a new methodology to classify the lesions by performing a pattern recognition step. The lesion is classified into five different types of patterns which are: reticular or network, globular, cobblestone, homogeneous, and parallel pattern. For analyzing the color textured pattern, they expressed the image as a finite symmetric conditional Markov (FSCM) model. They calculated a feature vector with the model parameters. They employed different color spaces and showed that the L*a*b* color space outperforms the others. To obtain the label assigning the type of the pattern, the maximum likelihood (ML) criterion was applied to maximize the conditional probability distribution. The inputs to the algorithm were 40×40 pixel images corresponding to a particular type of pattern, and the output was the class of such pattern. It is a supervised method due to the availability of a training set. The correct classification rate achieved was of 90% for the reticular pattern (pigment network) and 86% on average.

In a recent work [12], Sadeghi et. al. proposed a graph-based method to classify and visualize pigment networks. They validated the method by evaluating its ability to classify and visualize the real dermoscopic images. The accuracy of the system was 92.6% in classifying images to two classes of *absent* and *present*.

2. Present Proposed Approach

The aim of our recent approach is to decide the *presence* or *absence* of pigmented network in a lesion image. The specific location of the PN structure within the image is to be found and visualized. Then, the image is classified according to the ratio of the PN presence. This work explores a novel modified Laplacian of Gaussian (LoG) approach which includes the following steps:

1. *Automatic segmentation* of the lesion is performed to focus the computation cost only on those necessary pixels belong to the lesion.
2. *Lesion image enhancement* is performed to highlight the texture features.
3. *The luminance channel* (Y-channel) is then extracted from the enhanced image.
4. *Sharp change* of intensity is detected using the Laplacian of Gaussian (LOG) filter. The result of this *edge detection* step is a binary image which is subsequently converted into a graph to find meshes or cyclic structures of the lesion. After finding loops or cyclic subgraphs of the graph, noise or undesired cycles are removed.
5. Another graph of the pigment network is created using the extracted cyclic structures.
6. *Pigmented network holes* are detected in this step based on their features.
7. According to the density of the PN graph, the given image is classified into *absent* or *present*.

In the following sections, each step of the present procedure is detailed.

3. Automatic Lesion Segmentation

Prior information about the common dermoscopic images during acquisition is very useful to simplify the automatic segmentation algorithm. We summarize them here:

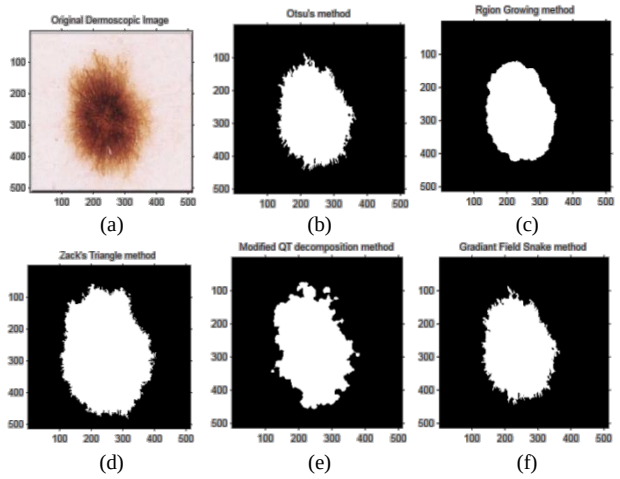

Figure 2: Five segmentation methods applied to the original dermoscopic image (a): Otsu (b); modified region growing (c); Zack's triangle (d); Quad-tree decomposition (e); and gradient field snake (f) methods.

1. There is only one region in the image to be segmented.
2. The region (or a part of it) is located around the center of the image.
3. The background is located at the image corners and edges.
4. The normal skin color, the background, is well-defined.
5. The illumination conditions during image acquisition are homogeneous with white light.
6. The lesion is always darker than the surrounding areas.

Considering the above information, we developed, applied, tested and compared five automatic segmentation algorithms, Figure 2: Otsu [13]; modified region growing [14]; Zack's triangle [15]; Quad-tree decomposition [16]; and gradient field snake [17] methods. Based on the results, these algorithms are manually compared to choose the closest one to the sixths manual segmentation.

For the color image we use the lossless compressed JPG image format. While for the black and white segmentation mask we prefer the BMP format. The reason is that BMP format presents only a true color of black and white without any deformation for the mask borders. Hence, an increase of the overall quality of our algorithm is obtained.

4. Lesion Sharpening and Y-Channel Extraction

The segmented lesion is further sharpened to highlight the texture features, Figure 3. A 3x3 contrast enhancement filter created from the negative of the Laplacian filter is applied. The filter parameter α in the range of 0.0 to 1.0 controls the shape of the Laplacian. The default value for alpha is 0.2.

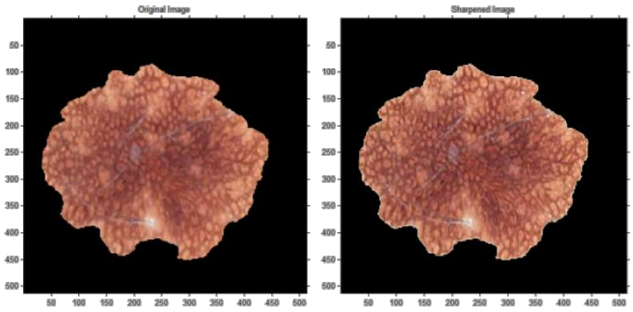

(a) (b)

Figure 3: (a) the original segmented lesion before sharpening. (b) the segmented lesion after applying the 3x3 contrast enhancement filter.

In a further step, the algorithm classifies only light and dark areas regardless of the color. Hence, only the luminance channel (Y) is considered and extracted from the color segmented image using the following equation:

$$Y = 0.299\ R + 0.587\ G + 0.114\ B$$

Where Y is the luminance and R, G and B are the red, green, and blue color components, respectively.

Color space conversion is not necessary in this step. So, to optimize the computational cost, we only use the luminance regardless the contents of other channels.

5. Feature Extraction

This step of the algorithm finds the holes in the lesion. It finds the holes belong to pigmented network and other structures as well. The presence of atypical PN is indicated by "black, brown, or gray network with irregular meshes and thick lines" and a typical PN is defined as a "light- to dark-brown network with small, uniformly spaced network holes and thin network lines distributed more or less regularly throughout the lesion and usually thinning out at the periphery". These structures show prominent lines, homogeneous or inhomogeneous meshes.

From an image processing point of view, these structures can be detected firstly by searching for the occurrence of the texture and consequently by evaluating its possible chromatic and spatial evolution. To extract these key features we search for round structures which represent the presence of the pigment network. To find the meshes' structures in the luminance image, it is necessary to detect sharp changes of the intensity.

Because of the inherent properties of Laplacian of Gaussian (LoG) filter, it can detect the "light-dark-light" changes of the intensity well.

$$\mathrm{LoG}(x,y) = -\frac{1}{\pi\sigma^4}\left(1-\frac{x^2+y^2}{2\sigma^2}\right)e^{\frac{-(x^2+y^2)}{2\sigma^2}}$$

The detection criterion is the presence of a zero crossing in the second derivative with the corresponding large peak in the first derivative.

$$h(x,y) = \Delta^2[g(x,y) * f(x,y)] = [\Delta^2 g(x,y)] * f(x,y)$$

$$\Delta^2 g(x,y) = \left(\frac{x^2+y^2-2\sigma^2}{\sigma^4}\right)^{\frac{-(x^2+y^2)}{2\sigma^2}}$$

Setting the threshold to zero, we obtain an edge image with closed contours of zero-crossings in the input image. The next step is to detect the meshes or round structures in the edge image.

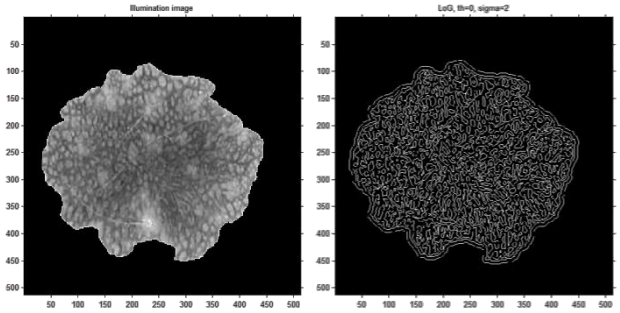

(a) (b)

Figure 4: (a) the original segmented lesion before Laplacian of Gaussian (LoG) filtering. (b) the detected holes based on connected components technique.

In previous work [8, 9], these structures are usually found by morphologic techniques and a sequence of closing and opening functions were applied to the black and white image. These methods are error-prone in detecting the round shape structures. So, the LoG filter detects the 8-connected neighbors,

Figure 4. Each pixel in the connected component is a node. Each node has a unique label according to its coordinates.

The network structure from the detected compound structure, holes belong to the meshes of PN, is then separated. The other detected structures (globules and dots) are removed according to the prior knowledge about the PN.

For every detected hole, the present algorithm performs this task as follows:

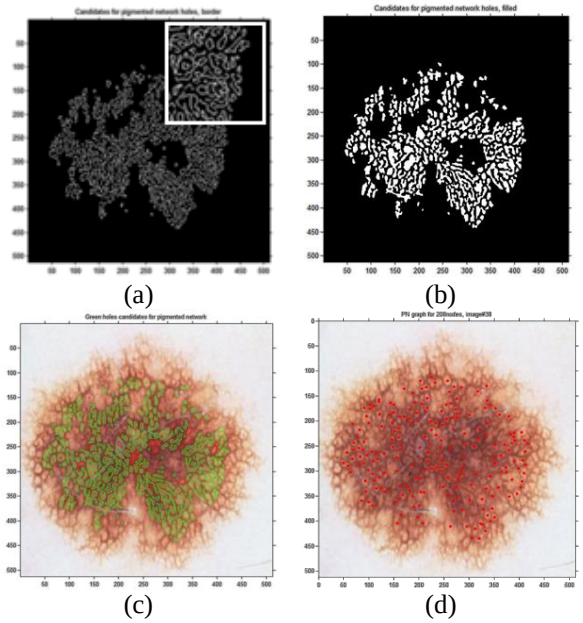

Figure 5 : (a) The generated mask to extract the border around each hole in the lesion (partially magnified). It is used to calculate the border average luminance value (B) around the hole. (b) the generated mask to extract the inner area of each hole. It is used to calculate the inner area average luminance value (N). (c) Original dermoscopic image with pigmented network classified with the green mask (Gmask). The red mask (Rmask) shows those holes belong to other structures of the lesion. (d) Original dermoscopic image with graph whose nodes are centers of the meshes belonging to the pigment network (centers of holes in the Gmask).

1. Thicken the 1-pixel wide border with 2 pixels. This provides higher pixel count to calculate the luminance of the surrounding area around the hole, Figure 5(a).
2. Calculate the average of the thickened border intensity (B) values.
3. Separate each hole as a mask to extract the luminance of its inner area, Figure 5(b).
4. Calculate the average intensity of the inner area (N).
5. If N is greater than B; the decision is taken that this single hole belongs to the pigmented network.

After classifying all of the detected holes, the algorithm generates two masks. The first mask we call green-mask (Gmask) that contains all the candidate holes belong to PN. The second mask we call red-mask (Rmask) that contains the rest of the holes belong to other structures. Figure 5(c) illustrates the two masks.

In order to visualize the graph of a PN, a new graph is created whose nodes are centers of the meshes belonging to it, Figure 5(d).

6. Localizing the Pigmented Network

Considering spatial arrangement of holes of the PN, their Euclidean distance is set to a threshold. Nodes within a an adaptive maximum distance threshold (AMDT) are connected together, instead of a constant maximum. We relate the AMDT to the average size of the holes in the pigmented network mesh (Gmask) as follows:

$$AMDT = 10\sqrt{\frac{A}{\pi}}$$

Where A is the average area of the holes, we approximate it as a full circle. A hole is considered belonging to a local PN area if it is connected with a distance of at most 10 times more of its radius to the neighboring holes.

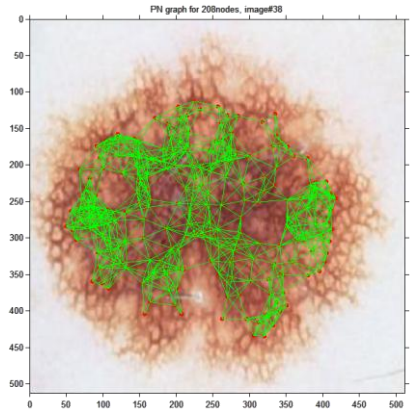

Figure 6: Original dermoscopic image with the complete graph whose nodes are centers of the detected meshes belonging to the pigment network. The edges represent the connections between the nodes within an adaptive maximum distance threshold AMDT.

Figure 6 illustrates both the nodes and the connections of the PN area. Each center of the meshes is considered vertex, or node. While each green line is considered an edge.

The total number of vertices (V) and the total number of connecting edges (E) both with the segmented lesion area size (S) indicate the presence or absence of the pigmented network in the lesion. Define the density (D) to be:

$$D = \frac{E}{V \log S}$$

Images containing a D ratio higher than a threshold (set to 1.2 in our study) are classified as present and the rest as absent. The dermoscopic image in Figure 6 is considered as present.

7. Discussion and Conclusion

We applied our method to a set of a 100 dermoscopic images adapted from *Atlas of Dermoscopy of Pigmented Skin Tumors* [18]. All of the dermoscopic images of this training set were labeled by the experts of the atlas to have malignant melanoma with pigmented network *present*. We tuned the parameters and thresholds of our proposed method according to this set.

Figure 7, shows a sample image matrix of our experimental results. It consists of three rows (a, b and c) and four columns (1 to 4). The first and third rows show a *present* pigmented network in the dermoscopic image. The second row represents the *absent* case. All of the three are classified correctly. Each column is arranged as follows:

1. The original dermoscopic image of the lesion under diagnosis

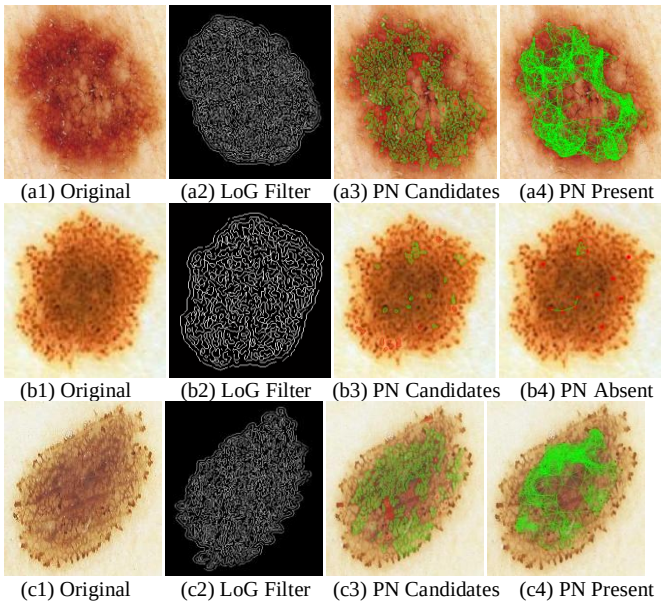

Figure 7: Sample experimental results from applying the present algorithm. The three rows and four columns in this figure are arranged as follows: Rows a, b, and c illustrates 3 different malignant cases. Column 1: the original dermoscopic image; Column 2, the binary edge-detected image after applying the LoG filter; Column 3: the candidate holes belong to pigmented network (PN), shown as a green mask; Column 4: the visualization of the pigment network with the connections. Rows a and c illustrate present pigmented network (PN). Row b illustrates absent PN.

2. The binary edge-detected image after applying the LoG filter.
3. The candidate holes belong to PN, shown as a green mask. The rest of the holes (not belonging to PN) are shown in red.
4. The visualization of the pigment network with the connections based on the AMDT threshold.

The accuracy of our pigment network detector is 70.8% for 100 images in the training set for the 2-class classification (*present* or *absent*).

We consider such accuracy as *low* compared to a relative work [12]. However, our definition of the maximum distance threshold (MDT) is more adaptive to take the biological structure of the lesion into account. Furthermore, extensive fine-tuning of the system parameters leads to high accuracy for a specific set of dermoscopic images. Therefore, the present approach is more flexible with an acceptable performance.

As a future work, we would like to consider five more aspects:

1. Define a method to combine the presented five segmentation algorithms into one optimum algorithm.
2. After the LoG filtering we would like to define and apply a selection rule for the size and shape of the PN meshes. We propose to ignore the 25% of both the highest and lowest size of the mesh areas.
3. We also recommend a shape classification based on a ratio between the major and minor axis of the enclosing ellipse around a mesh. The closer this ratio to "one", the more probable the mesh would belong to our targeted structure.
4. To identify PN holes, we propose to use a border segmentation similar to that used in our B-Scoring algorithm (published as internal report). This would be computationally very expensive but still more accurate.
5. The Rmask, classified meshes not belonging to PN, can be further investigated to as being globules.

The present model is a part of a complete system based on the ABCD rule that targets for a reliable intelligent dermatoscope for melanoma diagnosis.

Acknowledgment: This work was supported in part by the Hungarian Scholarship Board.

References

[1] Marchesini R, Bono A, Bartoli C, Lualdi M, Tomatis S and Cascinelli N: Optical imaging and automated melanoma detection: question and answer. Melanoma Res 12(3): 279-286, 2002.

[2] Friedman, R. J., Rigel, D. S., and Kopf, A. W., "Early detection of malignant melanoma: the role of the physician examination and self examination of the skin," CA Cancer J Clin 35, 130–151, May 1985.

[3] Menzies, S. W., "A method for the diagnosis of primary cutaneous melanoma using surface microscopy,"Dermatologic Clinics 19, 299–305, 2001.

[4] Ilias Maglogiannis and Charalampos N. Doukas, "Overview of Advanced Computer Vision Systems for Skin Lesions Characterization", IEEE transactions on information technology in biomedicine, vol. 13, no. 5, September 2009.

[5] Yadav, S., Vossaert, K. A., and Kopf, A., "Histopathologic correlates of structures seen on dermoscopy (epiluminescence microscopy)," Am J Dermatopathol 15, 297–305, 1993.

[6] Massi, D., De Giorgi, V., and Soyer, H. P., "Histopathologic correlates of dermoscopic criteria," Dermatologic Clinics 19, 259–268, 2001.

[7] Soyer, H. P., Argenziano, G., Chimenti, S., and et al., "Dermoscopy of pigmented skin lesions: Results of a consensus meeting via the internet," Journal of the American Academy of Dermatology 48(5), 679–693, 2003.

[8] Anantha, M., Moss, R. H., and Stoecker, W. V., "Detection of pigment network in dermatoscopy images using texture analysis," Computerized Medical Imaging and Graphics 28, 225–234, July 2004

[9] Betta, G., Di Leo, G., Fabbrocini, G., Paolillo, A., and Sommella, P., "Dermoscopic image-analysis system: estimation of atypical pigment network and atypical vascular pattern," in [MEMEA '06: Proceedings of the IEEE International Workshop on Medical Measurement and Applications], 63–67, 2006.

[10] Grana, C., Cucchiara, R., Pellacani, G., and Seidenari, S., "Line detection and texture characterization of network patterns," in [ICPR '06: Proceedings of the 18th International Conference on Pattern Recognition],

275–278, IEEE Computer Society, Washington, DC, USA, 2006.
[11] Serrano C., and Acha, B., "Pattern analysis of dermoscopic images based on markov random fields," Pattern Recogn. 42(6), 1052–1057, 2009.
[12] M. Sadeghi, M. Razmara, M. Ester, T. K. Lee and M. S. Atkins, "Graph-based pigment network detection in skin images", Proc. SPIE 7623, 762312, 2010.
[13] N. Otsu, "A Threshold Selection Method from Gray-Level Histograms," IEEE Transactions on Systems, Man, and Cybernetics, pp. 62-66, Vol. 9, No. 1, 1979.
[14] V. Vezhnevets, V. Konouchine "'GrowCut' – InteractiveMulti-Label N-D Image Segmentation By Cellular Automata".Graphicon-2005, Novosibirsk Akademgorodok, Russia, 2005.
[15] Zack GW, Rogers WE, Latt SA, "Automatic measurement of sister chromatid exchange frequency", J. Histochem. Cytochem. 25 (7): 741–53, 1977.
[16] Raphael Finkel and J.L. Bentley, "Quad Trees: A Data Structure for Retrieval on Composite Keys". Acta Informatica 4 (1): 1–9, 1974.
[17] Shawn Lankton, "Sparse Field Methods-Technical Report", Georgia Institute of Technology, April 2009.
[18] Atlas of dermoscopy of pigmented skin tumors, http://www.pless.fr/dermatoscopie/, 2011

Ahmed Ayoub is an assistant professor at Benha University, Egypt. He received his PhD in optical computing from faculty of electrical engineering and informatics, Budapest University of technology and economics, Hungary, 2005.
He joined the analogic and neural systems laboratory, computer and automation research institute (SZTAKI) in Budapest, 2000-2008. Now he is a visiting assistant professor of computer science at Shaqra University, Saudi Arabia. His recent research interests are: image processing for melanoma diagnosis, digital holographic microscopy and 3D target tracking.

András Hajdu is an associate professor at the University of Debrecen, Hungary, where he received his PhD in 2003. He has authored or co-authored 18 journal papers and 62 conference papers. His main interest lies in discrete mathematics with applications in digital image processing.